Effective Two-Photon Absorption Cross Section of Heteroaromatic Quadrupolar Dyes: Dependence on Measurement Technique and Laser Pulse Characteristics

Raffaella Signorini,[†] Camilla Ferrante,[†] Danilo Pedron,[†] Michele Zerbetto,[†] Elio Cecchetto,[†] Matteo Slaviero,[†] Ilaria Fortunati,[†] Elisabetta Collini,[†] Renato Bozio,*[,†] Alessandro Abbotto,[‡] Luca Beverina,[‡] and Giorgio A. Pagani[‡]

Department of Chemical Science and INSTM, University of Padova, Via Marzolo 1, I-35131 Padova, Italy, and Department of Material Science and INSTM, University of Milano-Bicocca, Milano, Italy

Received: December 2, 2007

The linear and nonlinear optical properties of the heteroaromatic push−pull−push two-photon absorbing dye *N*-methyl-2,5-bis[1-(*N*-methylpyrid-4-yl)ethen-2-yl]-pyrrole ditriflate (PEPEP) are reported. The determination of the two-photon absorption (TPA) cross-section spectrum has been performed with different techniques: femtosecond TPA-white light continuum probe experiments, two-photon-induced fluorescence, and open aperture Z-scan measurements using both nanosecond and femtosecond laser pulses. The measured TPA cross sections and their wavelength dispersion show a marked dependence on the parameters of the laser pulses and on the measurement technique employed. These properties are discussed in terms of the different microscopic mechanisms that can contribute to the multiphoton absorption processes, with different weight depending on the measurement conditions and on the photophysical parameters of the dye.

Introduction

The study of the two-photon absorption (TPA) properties of new materials is a very active research area because of their usefulness in a number of technological applications. For instance, they can be used for optical data storage,[1] multiphoton fluorescence microscopy,[2] and optical limiting purposes.[3] In recent years, the structure−property relations governing TPA have been studied extensively both experimentally and theoretically. The synthetic work has been focused on molecules of growing complexity: from simple dipolar to quadrupolar and octupolar dyes to dendrimers. The TPA cross sections and their wavelength dispersion have been measured by using a variety of two-photon techniques and experimental arrangements. Theoretical and computational methods have been optimized in order to identify guidelines for the synthesis of molecules with high TPA capabilities and to calculate TPA cross sections with increasing accuracy. All of these combined efforts yielded a wealth of novel results on the design and development of very efficient TPA dyes.[4]

One design strategy required to access molecules with large TPA activities involves symmetrically substituted systems having a general structure of the type D-π-D or the complementary structure A-π-A, where A is an acceptor group, D is a donating group, and π is a conjugated bridge. In these molecules, a symmetrical charge transfer takes place from the end-capped moieties toward the central π bridge. Intramolecular charge transfer can be further increased in systems having a general structure of the type D-π-A-π-D or A-π-D-π-A, leading to even more efficient systems.

The majority of efficient TPA dyes now available are based on substituted conjugated benzene rings and rely on the electronic properties of primary organic simple functionalities such as amino or alkoxy groups.[5] A different group of efficient TPA dyes is based on the use of heteroaromatic compounds, where the A groups are pyridine, quinoline, and benzothiazole rings among the powerful electron-acceptor heteroaromatic rings, while the D group is a pyrrole ring, one of the strongest π-electron-donor groups among the five-membered monoheterocycles.[6] Furthermore, the intrinsic chemical versatility of the heteroaromatic rings makes these systems particularly appropriate in order to finely tune electronic and optical properties. The precious electronic properties of heteroaromatic rings have already been employed successfully for the design of efficient push−pull derivatives for second- and third-order nonlinear optical (NLO) activity.[7] We have recently reported the design of new heterocycle-based push−pull dyes[8] and prepared new highly efficient NLO-phores with large second-order NLO activity[9] or for frequency-upconverted lasing applications.[10]

The advantage of quadrupolar donor−acceptor dyes over dipolar ones is ultimately related to the presence of two low-lying electronic excited states having a charge-transfer (CT) character and large transition dipole moments, instead of only one such states in dipolar dyes. A simplified modeling of quadrupolar dyes shows that, for optimal TPA efficiency, the energy of the one-photon allowed (odd) CT state should lie close to midway between those of the ground and two-photon (even) CT state.[4] This situation is neither easy to achieve in real systems nor desirable. In fact, under those circumstances, the laser pulses that trigger the TPA process would be strongly attenuated by ordinary linear absorption and an essential feature of TPA, required in most applications, that is, optical transparency at the laser wavelength, would be lost. Indeed, even the closeness of one-photon resonances, besides providing a mechanism for TPA enhancement, implies that multiphoton processes other than coherent, instantaneous TPA may occur and make the overall multiphoton process less unambiguous, with particular regard to its wavelength dispersion, dynamics, and dependence on laser pulse duration and intensity.

* Author to whom correspondence should be addressed. E-mail: renato.bozio@unipd.it.
[†] University of Padova.
[‡] University of Milano-Bicocca.

10.1021/jp7113779 CCC: $40.75
Published on Web 04/02/2008

SCHEME 1: Chemical Structure of the TPA Dye PEPEP

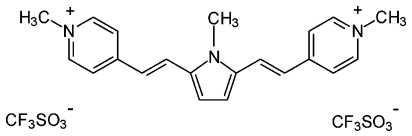

In this paper we present the results of our TPA study of the heterocycle-based two-photon dye *N*-methyl-2,5-bis[1-(*N*-methylpyrid-4-yl)ethen-2-yl]-pyrrole ditriflate (hereafter denoted as PEPEP, Scheme 1). The synthesis and some preliminary data on the TPA-based optical limiting activity of PEPEP have already been reported.[11] We herein report a complete linear and nonlinear optical characterization in a wide wavelength range. We provide detailed measurements of the TPA and multiphoton absorption properties for both femtosecond and nanosecond laser pulses and discuss the results obtained with particular attention to the TPA cross sections measured with pulses of different time duration (τ_L) and with different measurement techniques.

The determination of TPA cross sections is generally performed with nonlinear (NL) transmission or open aperture Z-scan techniques,[12] based on the use of femtosecond (fs) or nanosecond (ns) pulses, with two-photon-induced fluorescence (TPIF) or with TPA-white light continuum probe (TPA-WLCP) technique based on fs pulses. The characteristics of the laser pulse, especially the pulse duration and its intensity, affect the value of the measured TPA cross sections. It is generally found that these values differ by more than 1 order of magnitude on going from ns to fs pulses.

By using pulses with different τ_L it is possible to discriminate between three main possible contributions to the observed TPA cross section: (I) pure coherent TPA, with a negligible population of excited states, (II) TPA giving rise to a population of the excited state (either the final state of the two-photon transition or a different one reached after internal conversion or intersystem crossing), followed by a sequential absorption of a third photon, (III) incoherent two-step TPA.[13] The first process is always present in TPA; it is a third-order nonlinear effect related to the coherent terms of the third-order susceptibility, $\chi^{(3)}$; the observed absorption coefficient depends linearly on the intensity of the laser pulse, as long as massive population transfer, producing saturation of the TPA transition, is avoided. The second process depends on the incoherent excited-state population created by TPA, followed by sequential absorption of a third photon from the same laser pulse. Formally, it is a fifth-order nonlinear effect related to $\chi^{(5)}$, including feeding terms among excited states; however, it depends on the fluence of the laser pulse as the build-up of excited-state population implies time integration within the pulse duration. The last effect is still a third-order effect that considers the possibility of populating the excited state through a pre-resonant one-photon process, followed by interaction with a second photon. This process depends on laser fluence as well.

Usually, sequential absorption processes should not contribute to the measured signal when fast fs pulses are employed. For this reason the measured TPA cross section, at low laser intensity, is mainly due to contribution I. Indeed, for the push−pull monomeric PRL-101 compound,[14] it was demonstrated that a purely coherent TPA cross section can be measured only with pulses shorter than 10 fs. Coherent three-photon absorption (a $\chi^{(5)}$ process) may also become observable when the intensity of the input laser becomes very large, but in that case the absorption coefficient will depend on the square of the laser intensity and the effective TPA cross section will show a linear dependence on it. The third contribution can play a role only when the excitation wavelength approaches the one-photon resonance, depending on many different parameters, such as the pulse duration and the excited-state lifetime.

When ns laser pulses are used, processes II and III can easily become dominant and lead to an effective TPA cross section ($\sigma_{TPA,eff}$) larger than that measured with fs pulses by more than 1 order of magnitude. That is because ns pulses of even moderate intensity carry a much larger fluence than fs ones; therefore, they are effective in building up incoherent excited-state population from which sequential one photon absorption occurs.[15,16]

Finally, the pulse wavelength position with respect to one-photon resonances has different effects with ns and fs pulses. With the fs pulses, when the laser wavelength approaches and eventually enters the one-photon absorption a monotonous increase of the σ_{TPA} is observed. This effect is inherent in a purely coherent TPA (process I) and is accounted for by a decreasing detuning in the one-photon resonance denominator in the third-order expression for σ_{TPA} (See appendix 1). With ns pulses, when the laser wavelength approaches the tail of the one-photon absorption, the population of the first excited state within the time envelope of the pulse may be relevant and may become dominant as the intermediate step in the overall two-photon process. This process may also be viewed as a form of reversed saturable absorption (RSA) in its incipient stage when an absorbing excited state is weakly populated.[3]

Experimental Section

PEPEP, whose synthesis has been already described,[11] was dissolved in pure anhydrous DMSO at $\sim 1 \times 10^{-5}$ M and at 3×10^{-2} M concentrations for the linear and nonlinear optical measurements, respectively.

The linear absorption and emission spectra of PEPEP were recorded with a Cary 5 spectrophotometer and a Perkin-Elmer LS50 fluorimeter, respectively. Measurement of the fluorescence quantum yield (Φ_{FL}) was done by comparison with perylene in cycloexane, whose Φ_{FL} is known. The fluorescence spectra of PEPEP and of the standard were recorded at two excitation wavelengths: 410 and 480 nm.

The TPA cross section of PEPEP was measured by means of open aperture Z-scan experiments performed with femtosecond and nanosecond laser sources, and by TPA-WLCP and TPIF experiments performed using femtosecond pulses.

Two different femtosecond laser sources have been used. The fist one (laser system 1) was an amplified Ti-Sapphire laser system (Spectra Physics) that delivers ~130 fs pulses, with 0.7 mJ pulse energy, at ~800 nm. By controlling the Pockels cells in the regenerative amplifier, the repetition rate was reduced to 100 Hz. When used without amplification, laser system 1 delivers pulses with a duration of ~80 fs, in the wavelength range from 750 to 850 nm, ~ 5 nJ pulse energy at 800 nm, with 82 MHz repetition rate. The second laser source (laser system 2) was also a Ti-Sapphire laser system (Coherent, mod. Mira Optima 900-F). It delivers pulses with ~130 fs duration, in the wavelength range from 700 to 1000 nm, with 76 MHz repetition rate and ~10 nJ pulse energy at 800 nm. The spatial profile of the input beam was measured using a CCD camera (Pulnix TM-7CN) placed at the beam focus. The temporal profile was measured through autocorrelation experiments in a type I BBO doubling crystal,[17] and the pulse energies were sampled with a pyroelectric detector (Molectron J3-05).

Z-scan measurements were performed with amplified laser system 1. The input beam was suitably attenuated by a set of neutral density filters and was focused with a 160 mm focal length lens onto a 1 mm thick optical cell mounted on a motorized translation stage (Newport M-UTM100P1HL with 5 μm resolution). The transmitted beam was focused onto a large area photodiode, whose signal was sampled by a 500 MHz oscilloscope (Tektronik TDS 520B).

The nanosecond laser source (laser system 3) was an excimer laser (Lambda Physik EMG102) pumped pulsed dye laser (Lambda Physik FL2002) operating with different dyes (LDS 690, LDS 759 and LDS 821) emitting 10 ns pulses in the wavelength range from 670 to 840 nm, with 1−10 Hz repetition rate. The laser beam was focused onto the sample, contained in a 1 mm thick optical cell mounted on a motorized translation stage (Newport M-UTM150CC1HL, 5 μm resolution, with MM2500 controller), using a 150 mm focal length lens. The incident and transmitted laser pulse energies were measured using photodiodes, whose signal was sampled by a BOXCAR integrator (SRS, Model SR280, Stanford). A personal computer stored the signal from the oscilloscope and from the Boxcar as a function of the sample position and controlled the motion of the translation stage. The spatial profile of the ns input beam was measured using a CCD camera (Pulnix TM-7CN) placed at the beam focus. The temporal profile was measured with a fast photodiode, and the pulse energies were sampled with a pyroelectric detector (Molectron J3-05).

Z-scan data were collected at 795 and 816 nm with the fs setup and in the 670−840 nm range with the ns setup. The open aperture Z-scan measurements were performed with input pulse energies in the 0.05−0.35 μJ range for femtosecond pulses and with energies in the 10−232 μJ range for the nanosecond ones.

The wavelength dispersion of the TPA cross section has been measured by TPA-WLCP experiments. The femtosecond laser beam (amplified laser system 1), with central frequency at 812 nm, was split into a pump beam and a weaker beam focused on a sapphire window to generate the white light continuum probe (500 ÷ 1100 nm). The IR pump and WLCP are crossed spatially and temporally on the sample. The intensity of the probe beam was kept well below the threshold for observing any detectable TPA from the probe beam alone. The attenuation of the probe beam was measured as a function of the time delay between pump and probe pulses. A positive delay indicates that the probe beam reaches the sample after the pump. The attenuation of the WLCP beam at zero delay is caused by a TPA process promoted by the simultaneous absorption of two photons, one from each of the two beams. The attenuation of the WLCP beam was recorded for 18 different wavelengths in the 600−1000 nm range, employing a 1×10^{-2} M solution of PEPEP in DMSO. The wavelength of the TPA spectrum is calculated as $\lambda_{TPA} = \lambda_{pump} \cdot \lambda_{probe}/(\lambda_{pump} + \lambda_{probe})$. The pump beam intensity and beam waist on the sample were set at ∼350 μJ and 1.5 mm, respectively, while the probe beam was at least 1000 times weaker and tightly focused. Data have been normalized with respect to the IR pump intensity.

The TPA cross section spectrum has also been measured by using the TPIF technique, with both femtosecond laser sources: laser system 1, not amplified in this case, and laser system 2. A portion of the fs beam was directed, by a beam-splitter, onto a photodiode, in order to detect the input intensity. The laser beam was collimated over the whole path length inside the 1 cm cuvette, by using a 400 mm focal length lens. The fluorescence was collected at right angle to the incident beam by using a lens ($f = 40$ mm) and detected with a photomultiplier tube (PMT). A computer-controlled oscilloscope recorded the fluorescence signal as a function of the input beam intensity, which was suitably controlled by a manually adjusted half-wave plate, in conjunction with a linear polarizer. Proper filtering elements (cutoff filters) were used between the sample and the PMT to prevent scattered laser light from reaching the detector. To reduce the path length of the fluorescence emission within the solution under study, and thus the effect of reabsorption, the incident beam was propagated as close as possible to the side window of the cell from which fluorescence was collected. The effect of reabsorption of the emitted light in these conditions (1 mm maximum distance between the collimated beam and the side window of the cuvette) can be quantified around 3% on the measured emission. Taking into account this low value, the data have not been corrected for reabsorption.

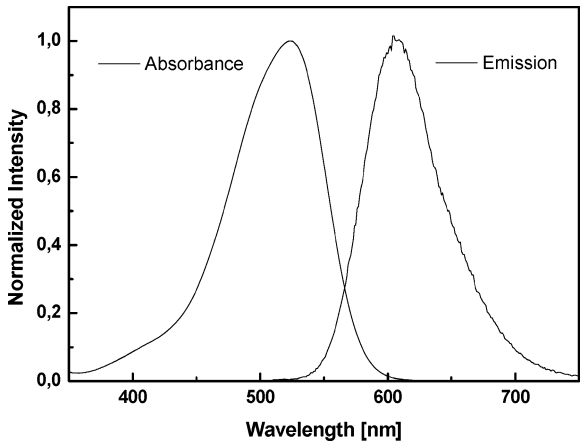

Figure 1. Absorption and emission spectra of PEPEP in DMSO, $C \sim 1 \times 10^{-5}$ M, 1 cm cell.

The TPIF measurements were done by comparison with fluorescein in water at pH = 11, whose two-photon properties have been well-characterized.[18] The fluorescence emission of the reference material, with a concentration of 1.3×10^{-4} M, and of PEPEP in DMSO, with a concentration of 4.2×10^{-5} M, were recorded in the 700−900 nm range (using a maximum input energy varying from 2 to 10 nJ) with laser system 1, and in the 750−850 nm range (using a maximum input energy varying from 1 to 5 nJ) with laser system 2. By checking the quadratic dependence of the fluorescence signal on the laser intensity in the whole wavelength range used for the TPIF measurements, the presence of a pure TPA process was verified in the 720−880 nm range with laser system 1 and in the 750−830 nm range with and laser system 2. In the other regions, deviations from quadratic behavior were observed.

Results

The absorption and fluorescence spectra of PEPEP are reported in Figure 1. PEPEP shows an absorption centered at 524 nm and an emission centered at 620 nm. A value of the fluorescence quantum yield $\Phi_{FL} = 0.14$ was determined for PEPEP by comparing the integrated area of the PEPEP fluorescence with that of the perylene standard.

Z-scan data with femtosecond and nanosecond pulses

Z-scan data are reported as normalized transmittance versus sample position (z) (i.e., as the ratio $I(z)/I(\infty)$, with $I(\infty)$ the linearly transmitted intensity far from the focal plane). The measurements were performed at 795 and 812 nm with fs pulses and in the 670−840 nm range with ns pulses. This wavelength range is far from the absorption peak of PEPEP (Figure 1). No

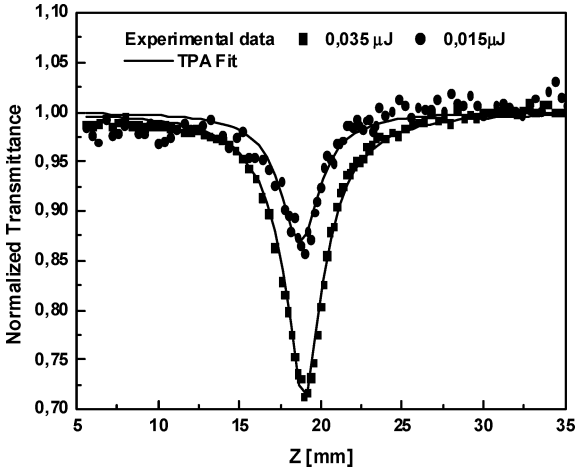

Figure 2. Z-Scan experimental data (points) and TPA fit (lines) of PEPEP in DMSO, in a 1 mm cell, with concentration of 3×10^{-2} M. Input pulse energy, of the fs laser, was 0.015 μJ (circles) and 0.035 μJ (squares).

signal occurs from the pure DMSO solvent even at the highest energies used, indicating that there is no nonlinear absorption contribution from the solvent.

Figure 2 reports the Z-scan data of PEPEP in DMSO, measured with fs pulses, at two different input pulse energies: 0.015 μJ (circles) and 0.035 μJ (squares). As expected, PEPEP solutions show a deep dip typical of nonlinear absorption, the depth of the dip being a linear function of the input energy.

Figure 3 shows the nanosecond open aperture Z-scan measurements performed with 178 μJ input pulse energy at different wavelengths: 690 nm (left side) and 720 nm (right side). Similar results were recorded at different wavelengths, ranging from 670 to 840 nm, and at different input energies.

The model used to fit the Z-scan data assumes a coherent two photon absorption process and was already discussed thoroughly in ref 12. The function describing the TPA processes, used to fit the Z-scan data is

$$T(z) = \sum_{m=0}^{\infty} \frac{-q_0(0)}{(m+1)^{3/2}} \frac{1}{1+(z/z_0)^m} \qquad (1)$$

where $q_0(0) = \beta I_0 L_{\text{eff}}$ is a parameter related to the TPA coefficient β, the intensity of the input beam I_0, and the effective length of the sample L_{eff}; z_0 is the Rayleigh range of the focusing optics. The molecular two-photon absorption cross section σ_{TPA}, is related to β through

$$\sigma_{\text{TPA}} = \frac{\hbar\omega\beta}{N_{\text{AV}}C} \qquad (2)$$

where N_{AV} is Avogadro's number and C is the concentration.

The full lines in Figure 2 are examples of the fit of the Z-scan data obtained by including up to the sixth order term in the summation of eq 1. Using this model, we obtain a good fit at both input energies. The parameters obtained from the fit of the Z-scan data for femtosecond pulses of energy 0.015 μJ and 0.035 μJ coincide within experimental error: $\beta = 0.08 \pm 0.01$cm^4/GW; $\sigma_{\text{TPA}} = (119 \pm 20) \times 10^{-50}$ cm^4·s/(photon·molecule). These measurements were repeated at least twice, on freshly prepared solutions, after a 6 month period and the σ_{TPA} value was confirmed and did not show any dependence on the input laser fluence. This, as well as the good fit to the shape of the Z-scan data, is consistent with the assumption that the basic mechanism for nonlinear absorption is either a coherent (instantaneous) or an incoherent (two-step) TPA process (contributions I and III, as described in the Introduction).

The nanosecond experimental data have been fitted (full lines in Figure 3) using the same function. However, in this case what we expect to get from the fitting is some kind of effective cross section, $\sigma_{\text{TPA,eff}}$. Table 1 reports the calculated cross sections at various wavelengths for different input energies. It

TABLE 1: TPA Cross Sections of PEPEP in DMSO at Different Wavelengths and Input Laser Intensity, Calculated from ns Z-scan Measurements

laser pulse λ (nm)	input laser intensity (μJ)	$\sigma_{\text{TPA,eff}}$ (cm^4 s/ph·mol) $\times 10^{50}$
670	11.40	13 480
670	21.93	72 299
680	47.81	11 826
680	128.95	12 804
680	134.21	16 277
690	128.95	5049
690	178.07	6275
690	232.46	9696
700	178.07	6345
700	232.46	7094
710	178.07	5602
720	178.07	3411
720	223.68	4947
820	131.58	3130
830	142.54	1139
840	122.81	2779

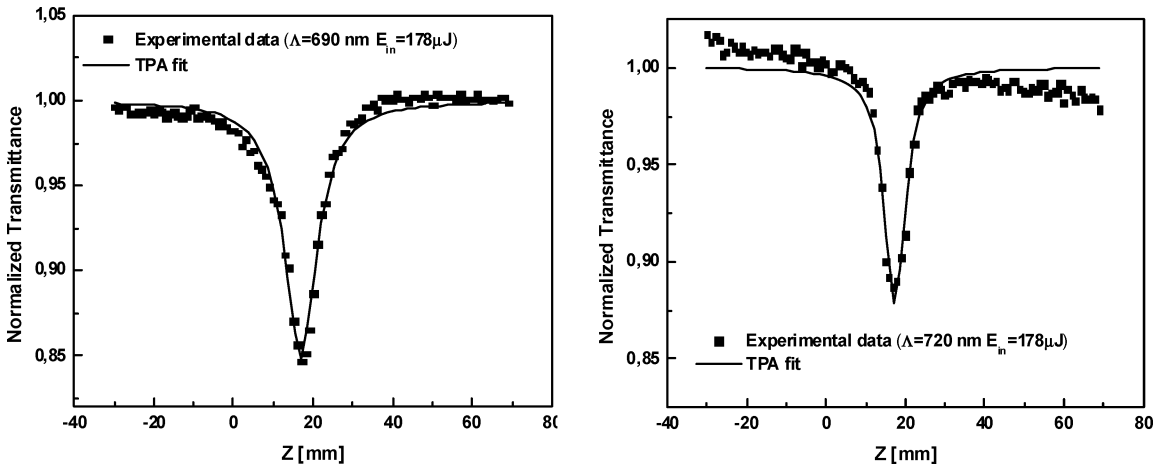

Figure 3. Z-scan experimental data (points) and TPA fitting (lines) of a 3×10^{-2} M solution of PEPEP in DMSO, in a 1 mm cell, performed with ns pulses with 178 μJ of energy, at 690 nm (left) and 720 nm (right).

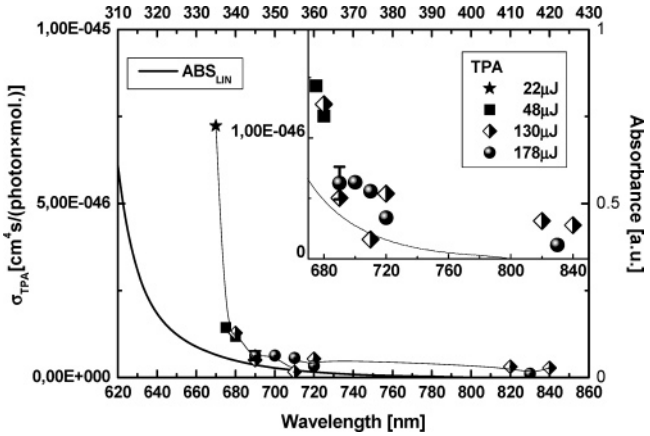

Figure 4. Wavelength dispersion of the TPA cross sections of PEPEP in DMSO, with $C = 3 \times 10^{-2}$ M, estimated from Z-scan measurements, performed by using ns pulses at different wavelengths, ranging from 670 to 840 nm, at different input energies.

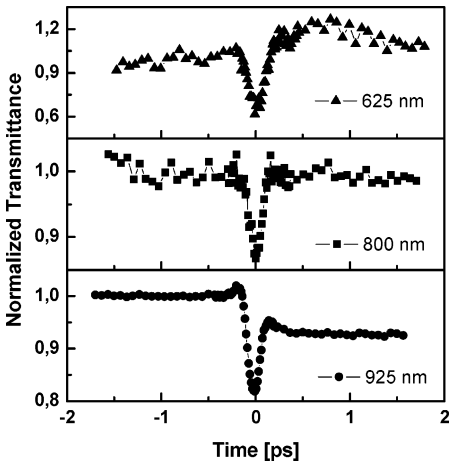

Figure 5. TPA-WLCP time traces measured at three different probe wavelengths, for 1×10^{-2} M PEPEP in DMSO with the same experimental conditions (i.e., same pump intensity and beam geometry).

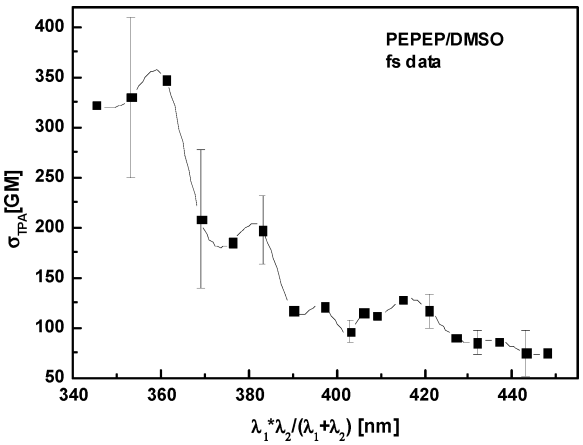

Figure 6. TPA spectrum of 1×10^{-2} M PEPEP in DMSO, measured with the TPA-WLCP technique, using 130 fs long pulses. The absolute value of the TPA absorption cross are expressed in GM; the wavelength scale indicates the position of the TPA peaks.

is apparent that the estimated $\sigma_{TPA,eff}$ values are intensity-dependent: the general tendency being to get larger values for higher pump intensities. The values estimated at 690 and 720 nm show a remarkable increase as the input laser intensity increases. This behavior can be understood considering that, with ns pulse duration, processes described as II in the Introduction, that is, sequential three- or multiphoton absorption, become relevant. Another important feature of Table 1 is the steep increasing value of $\sigma_{TPA,eff}$ at wavelengths shorter than 690 nm even though decreasing values of input pulse intensity have been used in the measurements. These values have been obtained at an intensity of the input beam 1 order of magnitude lower than the one used at longer wavelengths, indicating the presence of a resonance with the one-photon allowed transition (process III).

The resulting nonlinear absorption spectrum is depicted in Figure 4, where the TPA cross section data at wavelengths longer than 690 nm have been reported for 48, 130, and 178 μJ input pulse energies. The data at 670 nm also include a measurement at a lower intensity of 21 μJ. Figure 4 clearly shows the steep increase of the TPA cross section at short wavelengths, where the laser enters the far tail of the one-photon ground-state absorption. Under these circumstances, mechanism III may become operative adding to the instantaneous TPA and, possibly, to the TPA-ESA. The error bar reported for the value at 690 nm has been estimated from four different measurements at the same input intensity, by calculating the difference between the lowest and the highest values.

TPA-WLCP Results. Figure 5 displays the TPA-WLCP time traces recorded at three different probe wavelengths for a solution 1×10^{-2} M of PEPEP in DMSO. The normalized transmittance $T(t)$ of the probe beam at all of the investigated wavelengths is computed from $I_{probe}(t)/I_{probe}$ ($t < 0$). All of the traces are measured in the same experimental conditions and with equal pump beam intensity, their shape and the asymmetry observed at positive delay time will be discussed below.

Figure 6 shows the TPA spectrum in the 345−450 nm range. The data points were measured experimentally by the TPA-WLCP technique while the full line is the results of sp-line interpolation provided as a visual aid. The error bars were computed by repeating the TPA-WLCP experiments 3 times over a 2 month period and are calculated from the minimum and maximum values obtained.

The TPA-WLCP technique has been employed in order to measure the dispersion of the TPA cross section of PEPEP with ultrashort laser pulses. This technique relies on the measure of the transmittance of the probe beam, when the IR pump and the WLCP beam are overlapped in time and space on the sample. Under suitable conditions (i.e., the transmittance of the probe beam depends linearly on the IR pump beam intensity and is independent of the probe beam intensity) the probe beam normalized transmittance (T_{probe}) at zero delay time (t) is directly proportional to the TPA coefficient β[19]

$$T_{probe}(t = 0) = 1 - \beta \times I_{pump} \times k \qquad (3)$$

where I_{pump} is the intensity of the pump beam and k is a parameter influenced by the geometry of the experiment. The σ_{TPA} values at the different probe wavelengths are obtained by normalization of the experimental data with respect to the values measured through a Z-scan experiments performed at 812 nm. Estimating absolute σ_{TPA} values from the TPA-WLCP data would yield a higher error because it requires the measure of a number of experimental parameters larger than the one required for the Z-scan technique.

The time traces of the normalized transmittance of the probe beam at different wavelengths are shown in Figure 5. At all wavelengths one notices a sharp attenuation of the probe beam at time $t = 0$, that is, when the pump and the probe beam are overlapped in time. The fwhm of the dip corresponds, within the experimental error, to the autocorrelation width of the laser

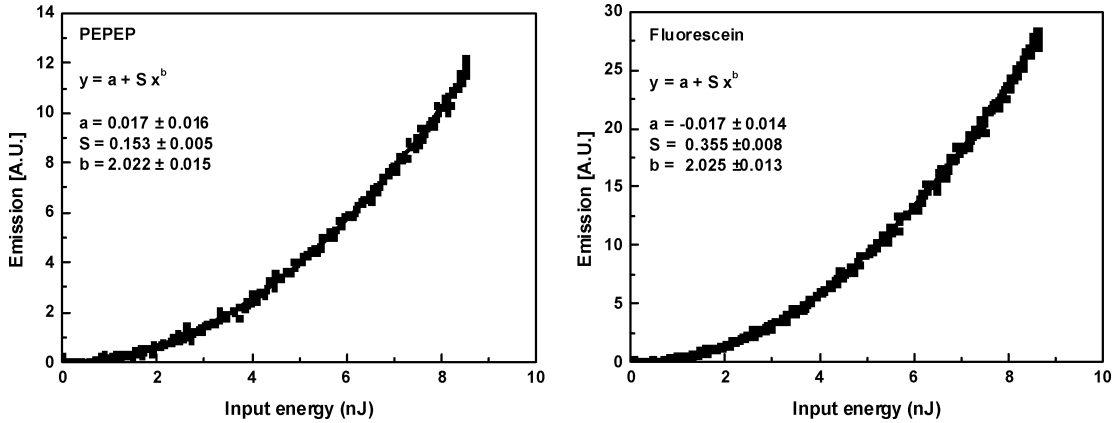

Figure 7. TPIF signal (squares) of PEPEP (left panel) and fluorescein (right panel) as function of the energy of the input beam, recorded at 780 nm. The fitting (lines) shows the quadratic dependence.

pulses measured with a BBO doubling crystal. Therefore, the attenuation of T can be attributed to an instantaneous TPA process. Furthermore, at 812 nm, it has been verified that the amplitude of the dip does not depend on the probe beam intensity, while it depends linearly on the IR pump beam intensity.

The behavior of T at positive delay time is different depending on the probe wavelength. In particular, at probe wavelengths shorter than 675 nm it is larger than the normalized transmittance. Between 675 and 925 nm T does not change before and after the application of the IR pump pulse. At wavelengths longer than 925 nm it is lower after the application of the IR pump pulse than before it. We attribute the deviations observed to a population process promoted by a TPA mechanism induced by the IR pump beam. The deviations of the transmittance at wavelength shorter than 675 nm is an indication that the molecules in the excited state absorb less than those in the ground state. The deviations observed at wavelengths longer than 925 nm points out that the absorbance of the excited-state molecules is larger than that in the ground state. At wavelengths in the 675−925 nm range it seems that the absorbance of the ground- and of the excited-state molecules are very similar and the amount of excited-state molecules produced by the TPA process is not enough to detect a signal related to the sequential excited-state absorption. Furthermore, measurements performed at 812 nm with increasing IR pump intensity do not show a variation in T at positive delays. Therefore, we expect that the excited-state population formed by a TPA process promoted by the IR pump pulse is indeed very small, and it is visible only when the absorption coefficients characterizing the ground and excited states are strongly different.

The TPA spectrum calculated from the time traces of the TPA-WLCP experiments is shown in Figure 6. As can be noticed, there is a shoulder at 415 nm followed by a continuous increase up to 360 nm, where a second maximum might be present. In order to confirm the presence of this peak, measurements should be extended at shorter wavelengths, but this is prevented by the strong linear absorbance of the sample at this wavelength. Because of the shape of the time traces for the TPA-WLCP experiments, we cannot exclude that the spectrum can be partly affected by sequential TPA processes; however, it is clear that an instantaneous TPA process dominates at time $t = 0$, that is, at the points used to calculate the TPA spectrum.

TPIF Data. The two-photon-induced fluorescence signals of PEPEP and fluorescein have been recorded in the wavelength range where TPA can be performed with our fs laser systems. Figure 7 reports the signal of PEPEP and fluorescein sampled at 780 nm, with laser system 2, as a function of the input intensity up to 9 nJ. The data of this figure show the pure emission from PEPEP and fluorescein because different contributions, coming from the cell or the solvents used, have already been subtracted from the experimental data. The full lines of Figure 7 represent the fitting of the experimental data by using the equation

$$y = a + Sx^b \tag{4}$$

The values obtained for the exponent b (2.022 for PEPEP and 2.025 for fluorescein) show a clear quadratic dependence of the emission signal on the input energy. A similar analysis of the experimental data of PEPEP and fluorescein has been performed at all wavelengths in order to discriminate data with quadratic dependence from the other.

The absolute σ_{TPA} values of PEPEP are calculated by comparing the TPIF emission of PEPEP with the emission of fluorescein, used as the standard, whose σ_{TPA} spectrum is known.[18] In this case it is possible to use the relation[20]

$$\sigma_{TPA,s} = \frac{S_s}{S_r} \cdot \frac{\Phi_{FL,r}\varphi_r C_r}{\Phi_{FL,s}\varphi_s C_s} \cdot \sigma_{TPA,r} \tag{5}$$

where $S_{s,r}$ is the curvature of the fluorescence signal as a function of the input energy (defined in eq 4 and shown in the inset to Figure 7), $\Phi_{FL,s,r}$ is the quantum yield of this emission process (assumed as 0.9 for fluorescein[18] and measured as 0.14 for PEPEP), $\varphi_{s,r}$ is the overall fluorescence collection efficiency, and $C_{s,r}$ is the molar concentration of the solution; the subscripts s and r refer to the sample and the reference solution, respectively. The value of $\varphi_{s,r}$ is related to the experimental apparatus, like the filters and the lenses used, the PMT response in the investigated wavelength range, and the refractive index of the solutions. Although the parameters related to the experimental apparatus are the same in going from fluorescein to PEPEP, it is necessary to take into account the difference of the refractive index of the solutions.[20]

Taking into account the value of $\Phi_{FL} = 0.14$, the action spectra ($\Phi_{FL} \times \sigma_{TPA}$ vs wavelength) measured with the different laser systems yield the σ_{TPA} dispersion curves reported in Figure 8. The figure shows σ_{TPA} values of PEPEP in the 100−800 GM range, with a maximum at about 820 nm that corresponds to a two-photon transition at 410 nm. Quite similar results have been obtained by repeating measurements with laser systems 1 and 2 that deliver 90 and 130 fs pulses, respectively.

Discussion

Let us discuss the various mechanisms that may contribute to the TPA data measured with different techniques and how

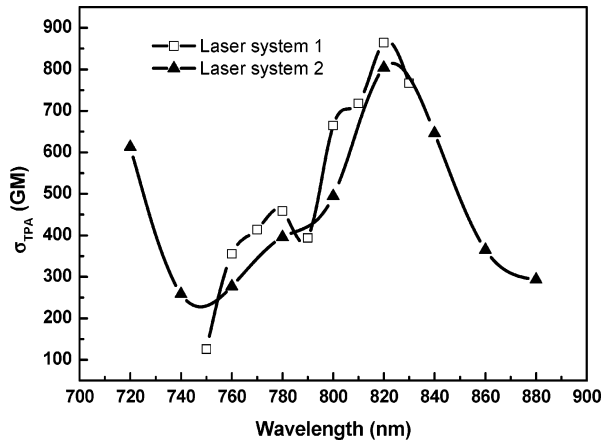

Figure 8. TPIF action spectra of PEPEP determined by the different fs laser systems.

they depend on optical and photophysical parameters of the system. A thorough analysis of the microscopic mechanisms contributing to multiphoton absorption processes and of their dependence on dynamical parameters of the material system and of the laser pulses has been reported by Gel'mulkhanov et al.[13] An effective multiphoton absorption cross section can be defined as

$$\sigma_{\mathrm{TPA}}^{\mathrm{eff}} = \sigma_1^{(2)} + \sigma_2^{(2)} + \sigma^{(3)}I \tag{6}$$

where $\sigma_1^{(2)}$ is the pure coherent TPA cross section (denoted as mechanism I in the Introduction section), $\sigma_2^{(2)}$ is the incoherent two-step (sequential) TPA (mechanism III), and $\sigma^{(3)}I$ is the contribution coming from a coherent TPA followed by absorption of a third photon (mechanism II). Perturbative expressions for the cross sections in eq 6 have been derived[13] with proper account of the population dynamics due to laser pumping, spontaneous decay, and feeding (i.e., internal conversion). In applying those expressions to PEPEP, we further assume the rotating wave approximation and consider that, being a quadrupolar structure, its π-electron system possesses inversion symmetry, implying that its excited states can be accessed either by one-photon or by two-photon transitions.

The first term in eq 6 takes up the usual form, generally used to describe TPA (explicit indication of the orientational averaging needed to describe processes in solution is omitted for simplicity)

$$\sigma_1^{(2)} = \frac{\omega}{c^2\epsilon_0{}^2\hbar^3}\frac{\Gamma_{i0}}{[(2\omega-\omega_{i0})^2+\Gamma_{i0}{}^2]}\sum_e \frac{\mu_{ie}{}^2\mu_{e0}{}^2}{(\omega-\omega_{e0})^2} \tag{7}$$

where ω_{mn}, μ_{mn}, and Γ_{mn} are the transition frequency, dipole moment, and dephasing rate of the $m \leftarrow n$ transition.

We focus on quadrupolar donor−acceptor structures that, for the purpose of describing TPA processes, can be modeled including a minimum of three electronic states. These include the ground state (0 subscript), a two-photon allowed state (i subscript), that corresponds to a symmetric intramolecular charge-transfer state, and an asymmetric charge-transfer state (α subscript), that lies at intermediate energy between the ground and the two-photon allowed state.

We account for the two-step TPA cross section, $\sigma_2^{(2)}$, in two limiting cases: (i) the steady-state limit whereby the laser pulse duration, τ_p, is much longer than the decay time of the intermediate state, $(1/\Gamma_\alpha)$; (ii) the short pulse limit, whereby $\Gamma_\alpha\tau_p \ll 1$.

At variance with the discussion presented in ref 13, we focus on the third and fourth term of their eq 15 because, in our case, they become the dominating ones both in the steady-state limit (because $\Gamma_\alpha/\Gamma_i \approx 10^{-3}$) and in the short pulse limit (because μ_{i0} vanishes for quadrupolar structures).

The effective TPA cross section for the two-step process can be cast in the simple form

$$\sigma_2^{(2)} \approx \frac{\omega\tau_{2-\mathrm{step}}}{c\epsilon_0{}^2\hbar^3}\sigma_{\alpha 0}(-\Delta)[\sigma_{i\alpha}(\Delta)-\sigma_{\alpha 0}(-\Delta)] \tag{8}$$

where $\sigma_\alpha 0(-\Delta)$ and $\sigma_{i\alpha}(\Delta)$ are the one-photon absorption cross sections for the transitions $\alpha \leftarrow 0$ and $i \leftarrow \alpha$, respectively, at a laser frequency ω detuned on opposite sides of the center frequency of those transitions by an amount $\Delta = |\omega_{\alpha 0} - \omega| = |\omega - \omega_{i\alpha}|$. In the long pulse (steady-state) limit, the characteristic time $\tau_{2-\mathrm{step}}$ equals the lifetime of the intermediate state τ_α, whereas in the short pulse limit it equals the pulse duration τ_p. Equation 8 emphasizes that the two-step TPA process where the intermediate state lies below the two-photon state basically corresponds to saturable or reverse saturable absorption depending on whether $\sigma_{i\alpha}(\Delta) < \sigma_{\alpha 0}(-\Delta)$ or $\sigma_{i\alpha}(\Delta) > \sigma_{\alpha 0}(-\Delta)$, respectively. An expression analogous to eq 8 can be obtained by integrating rate equations where NL absorption of a laser beam occurs starting from fluence-dependent populations in the ground state and in an excited state populated by one-photon absorption.

Comparing the cross section for the one-step coherent TPA, $\sigma_1^{(2)}$ in eq 7, with that for the two-step sequential TPA, $\sigma_2^{(2)}$ in eq 8, is not easy without resorting to numerical simulations. However, we can work out a sort of rule of thumb by manipulating eqs 7 and 8 to get

$$\frac{\sigma_2^{(2)}}{\sigma_1^{(2)}} \approx \Gamma_{\alpha 0}\tau_{2-\mathrm{step}}\left[\frac{\Gamma_{i0}\Gamma_{i\alpha}}{\Delta^2} - \frac{\Gamma_{i0}\Gamma_{\alpha 0}}{\Delta^2}\left(\frac{\mu_{\alpha 0}}{\mu_{i\alpha}}\right)^2\right] \tag{9}$$

For the specific case we are considering, that is, a quadrupolar dye with inversion symmetry and a one-photon allowed state lying below the two-photon state, eq 9 shows that the two-step TPA mechanism adds or subtracts to the coherent one-step process depending mainly on the ratio $(\mu_{\alpha 0}/\mu_{\alpha i})$. In most cases, this ratio is smaller than one because dipole moments for transitions starting from an excited state are greater than those starting from the ground state; hence, we expect the quantity in square brackets to be positive. In the long pulse limit, $\Gamma_{\alpha 0}\tau_{2-\mathrm{step}} = \Gamma_{\alpha 0}\tau_\alpha \gg 1$ because the dephasing time for a room-temperature dye is much faster than the decay rate of the lowest excited state. Hence, if the detuning from one-photon resonance is not much greater (2 orders of magnitude or more) than the width of the lowest absorption band, then the two-step sequential TPA will prevail over the coherent one-step TPA when using long pulses $(\tau_p/\tau_\alpha \gg 1)$. Indeed, for the two-step process to become negligible one would need to satisfy the condition $\Gamma_{\alpha 0}\tau_p \ll 1$, which is a very stringent requirement because the dephasing time in room-temperature solutions can be on the order of a few tens of femtoseconds.

For the description of the sequential process in which coherent TPA is followed by the absorption of a third photon (mechanism II), we need to go beyond the essential three-state model and to consider other states at energies higher than the two-photon state i. Let us denote one of these states as β and assume that the orientational averaging implied in the NL response of the system at fifth order of perturbation (needed to describe a three-photon absorption process)[13] can be decoupled into separate ones

for the TPA and for the subsequent one-photon absorption. Then, in the long pulse (steady-state) limit, we get

$$\sigma^{(3)} \approx \frac{\tau_i}{2} \sigma_1^{(2)} \sigma_{\beta i}(\Delta') \tag{10}$$

where $\sigma_{\beta i}(\Delta')$ is the one-photon absorption cross section for the $\beta \leftarrow i$ transition at a detuning Δ' of ω from exact resonance. In the short pulse limit the expression for $\sigma^{(3)}$ would scale down by a factor $\tau_p/\tau_i \ll 1$ with respect to eq 10. The contribution of sequential three-photon absorption to the measured σ_{TPA}^{eff}, eq 6, introduces a linear dependence on the pulse irradiance but is much smaller in the short than in the long pulse limit. It is worth mentioning that when using long pulses the absorption of the third photon may start from a state different from the two-photon state *i*, which is reached through nonradiative processes like internal conversion or intersystem crossing. Of course, the characteristic time of the nonradiative process would enter into the picture and the expression for $\sigma^{(3)}$ would turn into one more complicated than eq 10.

By comparing the values and the wavelength dispersion of σ_{TPA} of PEPEP (Table 1 and Figures 4, 6, and 8) one sees that the effective TPA cross sections measured with nanosecond pulses are more than 1 order of magnitude greater than those measured with fs pulses. According to the foregoing discussion, σ_{TPA} values measured using fs pulses are attributed mainly to instantaneous TPA, although using 150 fs pulses the contribution from $\sigma_2^{(2)}$ may still be non-negligible. Fifth-order effects can also be excluded because we did not observe a linear dependence of the TPA cross section on the pulse intensity. With the ns pulses, instead, there is a clear dependence of the measured σ_{TPA} on the laser intensity; therefore, this experimental data is strongly influenced by fifth-order processes. In conclusion, the main contribution to the large value of $\sigma_2^{(2)}$ measured with ns pulses comes from processes II and III, that is, from sequential TPA and from three-photon absorption.

The overall behavior of the spectra measured with ns and fs pulses shows an increase of the TPA cross section with decreasing wavelengths. This is well understood on the basis of the preresonance effect, that is, the influence of the one photon resonance when the pumping wavelengths approaches the one-photon allowed transition.[21] Note, however, that even considering purely coherent effects the preresonance enhancement is strongly dependent on the experimental technique employed (see Appendix 1 and the discussion below). With ns pulses the proximity of the one-photon resonance also implies an effective transfer of population to the first excited state and promotes further sequential absorption, according to the mechanism of eq 8.

If one looks at the fine structure of the three spectra measured by ns Z-scan, fs TPA-WLCP and TPIF (Figures 4, 6, and 8, respectively), then it is possible to observe different behaviors. Althoughthe ns dispersion does not show relative maxima, the fs ones display a different structure: the TPA-WLCP spectrum shows one peak at 415 nm and two shoulders at 380 and 355 nm, respectively, and the TPIF spectrum shows a clear maximum at 410 nm. The peak at 415 nm is larger than the experimental error, while the two shoulders are less clear because of the high noise affecting the data. All of the peaks fall at wavelengths shorter than the one-photon absorption maximum at 524 nm, consistent with the essential state model for quadrupolar molecules that exhibit TPA states at energies higher than the one-photon allowed state. PEPEP is a quadrupolar structure but indeed it lacks inversion symmetry, possessing a V-shaped molecular structure. A simple theoretical model[22] for a noncentrosymmetric V-shaped molecule with a quadrupolar charge distribution predicts the presence of two main transitions. The lower energy one is strongly one-photon allowed and shows a low TPA cross section, while the opposite is true for the high-energy one. If one looks at the one-photon absorption spectrum, then at 410 nm there is indeed a shoulder that we attribute to the same resonance observed in the TPA spectra. The different shapes displayed by the TPA-WLCP and the TPIF spectra can be related to the different wavelengths involved in the TPA process. Although the TPIF experiment is promoted by two photons possessing the same energy, in the TPA-WLCP setup the pump beam is fixed at 812 nm and the probe one varies in the 600−1000 nm range. When pulses with wavelengths lower than 760 nm are used, the presence of coherent pre-resonant effects may contribute to the nonlinear absorption, by enhancing it. This is clearly evident in the TPA-WLCP spectrum and starts to be seen in the TPIF spectrum as well.

The discrepancy between the absolute values of the σ_{TPA} measured with the two fs techniques, TPA-WLCP and TPIF, cannot be justified by the error bars associated with the measurement. The TPA-WLCP data are normalized with respect to the Z-scan data at 812 nm, and this value was established after repeated measurements. Also the TPIF data were repeated as shown above with different experimental setup and the calculation of the absolute σ_{TPA} are normalized with the literature data on fluorescein by Xu and Webb (ref 18), being the most widespread standard for this kind of measurements.

The fact that by using 130 fs pulses there still remains the possibility that two-step processes, mechanism III, partially contribute to the σ_{TPA} measured through the TPA-WLCP experiments cannot provide a satisfactory explanation for the discrepancy with the TPIF results. In both types of experiment there is convincing evidence that mechanism II, sequential three-photon absorption, does not contribute. Furthermore, the TPIF signal is not affected by the absorption of a third photon from the state populated by TPA as long as the decay from the upper state to the fluorescent state is fast compared with the fluorescence decay time. Provided that the use of different sample concentrations and pulse energies does note affect our results, which should be the case because we stayed well away from saturation conditions in both types of experiment, we would expect that the cross-section values measured with the two techniques should coincide.

The TPIF technique has recently been the subject of some controversy in the literature.[23] The technique is highly sensitive compared with the Z-scan method; however, it suffers from uncertainties arising from calibration of the measurement (e.g., the determination of the collection efficiency and of the fluorescence quantum yield) or from the choice of a suitable reference for standardization. Having chosen to use a standard for our measurement, the latter choice was critical. Fluorescein was the most appropriate choice, and we resorted to the value of σ_{TPA} reported by Xu and Webb.[18] Those authors reported σ_{TPA} values for other dyes as well, but some of those values have been questioned in more recent works. In the light of these considerations, we believe that the value obtained at 800 nm estimated for PEPEP by the Z-scan technique is more accurate and those at other wavelengths should be obtained by scaling the data as in Figure 6. Nonetheless, the TPIF method provides information on the wavelength dispersion of σ_{TPA} that bears a clearer indication of TPA resonances not obscured by one-photon preresonance effects.

Concluding Remarks

The optical characterization of PEPEP, a representative member of a new class of heterocyclic chromophores, was performed in order to study the influence of the laser pulse duration on its nonlinear optical properties. To this end, the value and wavelength dispersion of the TPA cross section was measured by using laser pulses of different time duration in the nano- and femtosecond range. The experiments were performed using three different techniques: Z-scan, TPIF, and TPA-WLCP.

First, a large difference between the absolute values of the TPA coefficients measured with fs pulses and ns ones was observed: ns TPA cross sections show values of σ_{TPA} more than 1 order of magnitude larger than those obtained with fs pulses. This fact can be explained by considering the effect of the different input pulse duration on the nonlinear response of the chromophore. The TPA obtained with fs pulses takes into account only instantaneous, coherent contributions, whereas the TPA cross section measured with long pulses is strongly affected by fluence-dependent processes such as off-resonant two-step TPA process and sequential three-photon absorption following pure TPA.

Regarding the overall behavior of the spectra measured with ns and fs pulses, an increase of the TPA cross sections with decreasing wavelengths was observed. This behavior was explained on the basis of the preresonance effect, considering the influence of the one-photon resonance when the pumping wavelength approaches the one-photon allowed transition. The ns spectrum does not show the presence of relative maxima, likely because of the overwhelming contribution of sequential multiphoton processes that are sensitive to the shape of the excited-state absorption spectra besides that of the TPA and one-photon absorption from the ground state (cf. eqs 8 and 10). The fs TPA spectra show a different behavior. The TPA-WLCP spectrum shows a resonance at 415 nm, while the TPIF spectrum shows a sharp maximum at 410 nm. These features have been attributed to a TPA transition showing a comparatively large cross section whereas it is observed as a weak shoulder in the one-photon spectrum, likely owing to the V shape of the molecule strictly lacking inversion symmetry. The increase of the fs σ_{TPA} in going to lower wavelengths is ascribed to a preresonance effect, more evident with the TPA-WLCP experiment than in the TPIF data.

The dye PEPEP is representative of TPA chromophores exhibiting relatively low-energy one-photon absorption in the visible region. Under these circumstances, the multiphoton processes may result from the superposition of several different microscopic mechanisms, the more so the longer the laser pulses compared to the characteristic times of the excited-state dynamics. Among the several applications of multiphoton processes in different areas of technology, optical limiting relies on a combination of linear and nonlinear optical properties to achieve the required device specifications: good transparency under low-level illumination, low threshold for nonlinear absorption, large dynamic range, high threshold for laser damage, wide spectral band of operation. Different materials choices and device architectures have been proposed to reach these goals based on RSA, TPA, or a combination of those mechanisms obtained by joining different materials.

The finding that a single chromophore may exhibit multiphoton processes resulting from an overlap of several mechanisms, especially when optically pumped by ns pulses, opens new perspectives to the design of functional molecules for optical limiting. In fact, close to one photon resonance the threshold for nonlinear transmission becomes lower, being dependent on a product of cross sections for one-photon (linear) absorption (eq 8). When the incoming pulse fluence becomes large, the TPA-ESA mechanism, eq 10, guarantees that the effective absorption cross section does not saturate, as is the case with the RSA mechanism.

Admittedly, the design of chromophores endowed with these properties remains a difficult task because it calls for the control of photophysical properties and excited-state dynamics of complex conjugated molecules. However, recent progress and further advances in computational methods and optical characterization techniques make this approach challenging but affordable.

Appendix A: Coherent One-Photon Pre-resonance Effect in TPA Spectra

The TPA process can be promoted by the instantaneous absorption of two photons of equal frequency ω_1 (degenerate TPA) or two photons with different frequencies: ω_1 and ω_2 (nondegenerate TPA). In both cases, the TPA cross section, $\sigma_{TPA}(\omega)$, at the lowest order of the perturbative approach, is directly related to the imaginary part of the third-order susceptibility $\chi^{(3)}$ by

$$\sigma_{TPA}^{D}(\omega_1) = \frac{3}{2}\frac{\hbar{\omega_1}^2}{c^2\epsilon_0 {n_1}^2 N}\,\mathrm{Im}\langle\chi^{(3)}(\omega_1,\omega_1,-\omega_1)\rangle \quad \text{(A.1)}$$

for the degenerate case and

$$\sigma_{TPA}^{ND}(\omega_2) = 3\,\frac{\hbar\omega_2\omega_1}{c^2\epsilon_0 n_1 n_2 N}\,\mathrm{Im}\langle\chi^{(3)}(\omega_1,|\omega_2,-\omega_1)\rangle \quad \text{(A.2)}$$

for the nondegenerate case. In these formulas $\hbar$ is the Plank's constant, c is the speed of light, n_i is the refractive index of the medium at the frequency ω_i, ϵ_0 is the vacuum dielectric constant, and N is the density of molecules.

An explicit expression for $\chi^{(3)}$ can be computed by means of the sum-over-states (SOS) formalism, in which the components of $\chi^{(3)}$ are defined on the basis of a density matrix defined on the molecular states.

Because the aim of this work is to write a simple expression that allows estimating explicitly the weight of the coherent one-photon preresonance effect on the degenerate and nondegenerate TPA spectra, the following assumption are applied:

(1) of the 48 terms contribuiting to the full expression of $\chi^{(3)}$, only the 16 resonant in a TPA process are considered.[24]

(2) on the basis of the rotating wave approximation, and the assumption that only coherent interactions are important, while the population terms are negligible, only four terms confer major contribution to the description of the TPA process and $\chi^{(3)}$can be written as[21]

$$\chi^{(3)}(\omega_1,\omega_2,-\omega_3) = \sum_{klmn} {\rho_{kk}}^0 \mu_{km}\mu_{mn}\mu_{nl}\mu_{lk} \cdot \left\{ \frac{1}{(\omega_{mk}-\omega_2-i\Gamma_{mk})(\omega_{nk}-\omega_2-\omega_1-i\Gamma_{nk})(\omega_{lk}+\omega_3-\omega_2-\omega_1-i\Gamma_{lk})} + \frac{1}{(\omega_{mk}-\omega_1-i\Gamma_{mk})(\omega_{nk}-\omega_1-\omega_2-i\Gamma_{nk})(\omega_{lk}+\omega_3-\omega_1-\omega_2-i\Gamma_{lk})} + \frac{1}{(\omega_{mk}-\omega_2-i\Gamma_{mk})(\omega_{nk}-\omega_1-\omega_2-i\Gamma_{nk})(\omega_{ln}-\omega_3+\omega_1+\omega_2+i\Gamma_{ln})} + \frac{1}{(\omega_{mk}-\omega_1-i\Gamma_{mk})(\omega_{ng}-\omega_1-\omega_2-i\Gamma_{nk})(\omega_{ln}-\omega_3+\omega_2+\omega_1+i\Gamma_{ln})} \right\} \quad \text{(A.3)}$$

where ρ^0_{kk} is the diagonal thermal-equilibrium density matrix element relative to the initally populated states k; μ_{ij}, ω_{ij}, and Γ_{ij} are the transition dipole moment, the transition frequency, and the HWHM relative to transition between states i and j; ω_1, ω_2, and ω_3 are the frequencies of the applied fields and the subscripts k, l, m, and n are dummy indices spanning the molecular states.

Furthermore if we suppose that

(3) the molecular system can be described adequately by a three-level system in which the molecular levels will be indicated by the subscripts g, e, and t, referring to the ground state, a one-photon allowed state, and a two-photon allowed state, respectively.

(4) in the sum of eq A.4, when the dummy index (k, l, m, n) is substituted with the real states index (g, e, t), only the resonant combination of indices makes a relevant contribution

(5) before the interaction with the applied field, all of the molecules are in their fundamental state so that $\rho^0_{gg} = 1$

then the expression for $\chi^{(3)}$ turns out to be

Degenerate Case.

$$\chi^{(3)}(\omega_1, -\omega_1,\omega_1) = 2\cdot\mu_{ge}\mu_{et}\mu_{te}\mu_{eg}\cdot \left\{\frac{1}{(\omega_{eg}-\omega_1-i\Gamma_{eg})^2(\omega_{tg}-2\omega_1-i\Gamma_{tg})}+\frac{1}{(\omega_{eg}-\omega_1-i\Gamma_{eg})(\omega_{tg}-2\omega_1-i\Gamma_{tg})(\omega_{et}+\omega_1+i\Gamma_{et})}\right\} \quad \text{(A.4)}$$

where for the system considered, it is always true that $\omega_{te} = \omega_{tg} - \omega_{eg}$.

In order to find a simple analytical formula for the imaginary part of $\chi^{(3)}$, in many papers the following approximations are also applied:

(6) the frequency of the applied field is chosen far enough from the one-photon resonant transition frequency so that $(\omega_{eg} - \omega_1) > (\omega_{tg} - 2\omega_1)$

(7) the HWHMs satisfy the conditions $(\omega_{eg} - \omega_1) > \Gamma_{eg}$ and $\Gamma_{te} \approx \Gamma_{eg}$

and the imaginary part of eq A.4 becomes

$$\mathrm{Im}[\chi^{(3)}(\omega_1, -\omega_1,\omega_1)] = \frac{2|\mu_{eg}|^2}{(\omega_{eg}-\omega_1)^2}\cdot\frac{|\mu_{et}|^2\Gamma_{tg}}{[(\omega_{tg}-2\omega_1)^2+\Gamma_{tg}^2]} \quad \text{(A.5)}$$

Substituting this expression in eq. A.1, we obtain

$$\sigma^{\mathrm{D}}_{\mathrm{TPA}}(\omega_1) \propto \frac{2|\mu_{eg}|^2}{(\omega_{eg}-\omega_1)^2}\cdot\frac{|\mu_{et}|^2\Gamma_{tg}}{[(\omega_{tg}-2\omega_1)^2+\Gamma_{tg}^2]} \quad \text{(A.6)}$$

This expression is often used to calculate the TPA degenerate spectra of organic chromophores measured with the TPIF technique. This formula is appealing because it allows one to separate the two-photon resonant term (second term on the rhs of eq A-6) from the so-called preresonance term (first term on the rhs of eq A.6).

TABLE 2: Parameters Used in the Simulation of Degenerate and Nondegenerate TPA[a]

ω_{eg} (10^{-15} s^{-1})	ω_{tg} (10^{-15} s^{-1})	ω_{te} (10^{-15} s^{-1})
3.625	4.542	0.917
(520 nm)	(415 nm)	(2055 nm)
Γ_{eg} ($10-15$ s^{-1})	Γ_{et} (10^{-15} s^{-1})	Γ_{tg} (10^{-15} s^{-1})
5×10^{-3}	2×10^{-2}	2×10^{-2}
μ_{eg}(10^{-29} cm)	μ_{tg}(10^{-29} cm)	μ_{te} (10^{-29} cm)
2.5	0	5.0

[a] The lifetimes of the excited states are kept equal.

Nondegenerate Case.

$$\chi^{(3)}(\omega_1, -\omega_1,\omega_2) = \mu_{ge}\mu_{et}\mu_{te}\mu_{eg}\cdot \left\{\frac{1}{(\omega_{eg}-\omega_2-i\Gamma_{eg})^2(\omega_{tg}-\omega_2-\omega_1-i\Gamma_{tg})}+\frac{1}{(\omega_{eg}-\omega_1-i\Gamma_{eg})(\omega_{tg}-\omega_1-\omega_2-i\Gamma_{tg})(\omega_{eg}-\omega_2-i\Gamma_{eg})}+\frac{1}{(\omega_{eg}-\omega_2-i\Gamma_{eg})(\omega_{tg}-\omega_1-\omega_2-i\Gamma_{tg})(\omega_{et}+\omega_2+i\Gamma_{et})}+\frac{1}{(\omega_{eg}-\omega_1-i\Gamma_{eg})(\omega_{tg}-\omega_1-\omega_2-i\Gamma_{tg})(\omega_{et}+\omega_2+i\Gamma_{et})}\right\} \quad \text{(A.7)}$$

Unlike the degenerate case, no further approximation can be applied, to extract a simple analytical formula from eq A.7, where the two-photon resonant term and the pre-resonant one are factorized.

Comparison of the Degenerate and Nondegenerate TPA Spectra. Equations A.4 and A.7 were used to simulate the TPA spectra in the degenerate and nondegenerate cases, respectively. The paramaters used for the three-level molecular model system are summarized in Table 2. As can be noticed, the chosen frequencies mimic the values observed for the molecule PEPEP studied in the present article, while the HWHM are similar to the values usually employed in the literature. The g→ e molecular transition dipole moment is computed from the absorption spectrum, the g → t one is assumed negligible, and the e → t one is chosen arbitrarily.

Figure 9 shows the TPA spectra in the degenerate (dashed line) and nondegenerate case (full line) obtained with the parameters of Table 2. The abscissa corresponds to the effective two-photon absorption wavelength (i.e., $\lambda = \lambda_1/2$ for the degenerate case and $\lambda = \lambda_1\lambda_2/(\lambda_1 + \lambda_2)$ for the nondegenerate one). As can be noticed, while the position of the TPA peak is

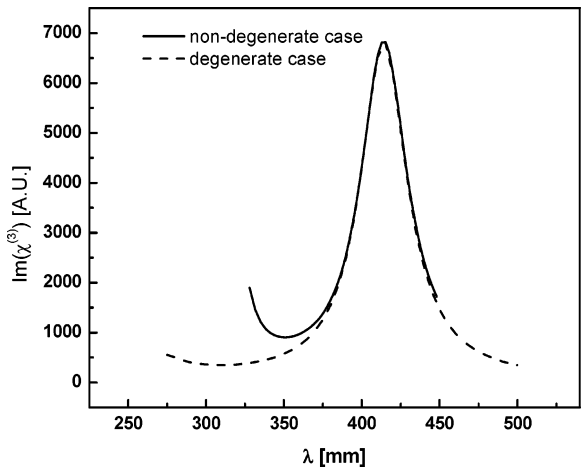

Figure 9. Calculated TPA spectra for the degenerate (dashed line) and nondegenerate (full line) experiment, for a three-level model system, whose parameters are summarized in Table 9.

similar for the two simulations, there is a steeper increase of the TPA cross section in the preresonance region for the nondegenerate spectrum with respect to the degenerate one. A similar behavior is observed in the experimental spectra of PEPEP. Therefore, the TPA-WLCP technique can turn out to be less efficient than the TPIF technique in detecting the TPA maxima if they fall at wavelengths in the nearby of the one photon resonance; nonetheless, it is a useful technique when nonfluorescent molecules are investigated.

Acknowledgment. We gratefully acknowledge financial support from the Italian Ministry for University and Research through the grants PNR-FIRB RBNE01P4JF and PNR-FIRB RBNE033KMA.

References and Notes

(1) (a) Parthenopoulos, D. A.; Rentzepis, P. M. *Science* **1989**, *245*, 843. (b) Cumpston, B. H.; Ananthavel, S. P.; Barlow, S. D.; Dyer, L.; Ehrlich, J. E.; Erskine, L. L.; Heikal, A. A.; Kueber, S. M.; Sandy Lee, I.-Y.; McCord-Maughon, D.; Qin, J.; Rockel, H.; Rumi, M.; Wu, X.-L.; Marder, S. R.; Perry, J. W. *Nature* **1999**, *398*, 51.

(2) (a) Denk, W.; Strickler, J. H.; Webb, W. W. *Science* **1990**, *248*, 73. (b) Belfield, K. D.; Bondar, M. V.; Przhonska, O. V.; Schafer, K. J.; Mourad, W. *J. Lumin.* **2002**, *97*, 141.

(3) (a) Proceedings of SPIE, *Nonlinear Optical Liquids and Power Limiters*; Lawson, Ed. **1997**, *3146*. (b) Proceedings of SPIE, *Nonlinear Optical Liquids and Power Limiters*; Lawson, Ed. **1998**, *3472*. (c) Proceedings of SPIE, *Nonlinear Optical Liquids and Power Limiters*; Lawson, Ed. **1999**, *3798*. (d) C. W. Proceedings of the First International Workshop on Optical Power Limiting **1999**, in *Nonlinear Optics*, *21*; Kajzar, F., Ed.; Gordon and Breach Science Publishers. (e) Proceedings of the Second International Workshop on Optical Power Limiting **2001**, in *Nonlinear Optics*, *21*; Bozio, R., Kajzar, F., Eds.; Gordon and Breach Science Publishers.

(4) (a) Albota, M.; Beljonne, D.; Bredas, J. L.; Ehrlich, J. E.; Fu, J. Y.; Heikal, A. A.; Hess, S. E.; Kogej, T.; Levin, M. D.; Marder, S. R.; Mccordmaughon, D.; Perry, J. W.; Rockel, H.; Rumi, M.; Subramaniam, C.; Webb, W. W.; Wu, I. L.; Xu, C. *Science* **1998**, *281*, 1653. (b) Reinhardt, B. A.; Brott, L. L.; Clarson, S. J.; Dillard, A. G.; Bhatt, J. C.; Kannan, R.; Yuan, L. X.; He, G. S.; Prasad, P. N. *Chem. Mater.* **1998**, *10*, 1863−1874. (c) Barzoukas, M.; Blanchard-Desce, M. *J. Chem. Phys.* **2000**, *113*, 3951.

(5) (a) Ehrlich, J. E.; Wu, X.-L.; Sandy Lee, I.-Y.; Rockel, H.; Marder, S. R.; Perry, J. W. *Opt. Lett.* **1997**, *22*, 1843. (b) Reinhardt, B. A.; Brott, L. L.; Clarson, S. J.; Dillard, A. G.; Bhatt, J. C.; Kannan, R.; Yuan, L.; He, G. S.; Prasad, P. N. *Chem. Mater.* **1998**, *10*, 1862. (c) Woo, H. Y.; Liu, B.; Kohler, B.; Korystov, D.; Mikhailovsky, A.; Bazan, G. C. *J. Am. Chem. Soc.* **2005**, *127*, 14721. (d) Woo, H. Y.; Hong, J. W.; Liu, B; Mikhailovsky, A., Korystov, D.; Bazan G. C. *J. Am. Chem. Soc.* **2005**, *127*, 820.

(6) Katritzky, A. R.; *Handbook of Heterocyclic Chemistry*; Pergamon Press: Oxford, 1983.

(7) Kuzyk, M. G.; Dirk, C. W., Eds. *Characterization Techniques and Tabulations for Organic Nonlinear Optical Materials*; Marcel Dekker: New York, 1998.

(8) (a) Abbotto, A.; Bradamante, S.; Pagani, G. A. *J. Org. Chem.* **2001**, *66*, 8883−8892. (b) Bradamante, S.; Facchetti, A.; Pagani, G. A. *J. Phys. Org. Chem.* **1997**, *10*, 514.

(9) (a) Abbotto, A.; Bradamante, S.; Facchetti, A.; Pagani, G. A. *J. Org. Chem.* **1997**, *62*, 5755. (b) Abbotto, A.; Facchetti, A.; Pagani, G. A.; Yuan, L. X.; Prasad, P. N. *Gazz. Chim. Ital.* **1997**, *127*, 165. (c) Abbotto, A.; Bradamante, S.; Facchetti, A.; Pagani, G. A.; Ledoux, I.; Zyss, J. *Mater. Res. Soc. Symp. Proc.* **1998**, *488*, 819. (d) Abbotto, A.; Beverina, L.; Bradamante, S.; Facchetti, A.; Klein, C.; Pagani, G. A.; Redi-Abshiro, M.; Wortmann, R. *Chem.—Eur. J.* **2003**, *9*, 1991−2007. (e) Archetti, G.; Abbotto, A.; Wortmann, R. *Chem.—Eur. J.* **2006**, *12*, 7151−7160.

(10) (a) Abbotto, A.; Beverina, L.; Bozio, R.; Bradamante, S.; Pagani, G. A.; Signorini, R. *Synth. Met.* **2001**, *121*, 1755. (b) Abbotto, A.; Beverina, L.; Bozio, R.; Bradamante, S.; Ferrante, C.; Pagani, G. A.; Signorini, R. *Adv. Mater.* **2000**, *12*, 1963.

(11) Abbotto, A.; Beverina, L.; Bozio, R.; Facchetti, A.; Ferrante, C.; Pagani, G. A.; Pedron, D.; Signorini, R. *Org. Lett.* **2002**, *4*, 1495.

(12) (a) Sheik-Bahae, M.; Said, A. A.; Wei, T.-H.; Hagan, D. J.; Van Stryland, E. W. *IEEE J. Quantum Electron.* **1990**, *26*, 760. (b) Wei, T. H.; Hagan, D. J.; Sense, M. J.; Van Stryland, E. W.; Perry, J. W.; Coulter, D. R. *Appl. Phys. B* **1992**, *54*, 46.

(13) Gel'mukhanov, F.; Baev, A.; Macak, P.; Luo Y.; Agren, H. *J. Opt. Soc. Am. B* **2002**, *19*, 937−945.

(14) Chung, S.-J.; Kim, K.-S.; Lin, T.-C.; He, G.-S.; Swiatkiewicz, J.; Prasad, P. N. *J. Phys. Chem. B* **1999**, *103*, 10741.

(15) Negres, R. A.; Van Stryland, E. W.; Hagan, D. J.; Belfield, K. D.; Schafer, K. J.; Przhonska, O. V.; Reinhardt, B. A. *SPIE* **1999**, *Vol. 3796*, 88.

(16) Swiatkiewicz, J.; Prasad, P. N.; Reinhardt, B. A. *Opt. Commun.* **1998**, *157*, 135.

(17) Sala, K. L.; Kenney-Wallace, G. A.; Hall, G. E. *IEEE J. Quantum Electron.* **1980**, *16*, 990.

(18) Xu, C.; Webb, W. W. *J. Opt. Soc. Am. B* **1996**, *13*, 481.

(19) (a) Shen, Y. R. *The Principles of Nonlinear Optics*; J. Wiley and Sons: New York, 1984. (b) Sutherland, R. *Handbook of Nonlinear Optics*; M. Dekker: New York, 1998.

(20) Rumi, M.; Ehrlich J. E.; Heikal, A. A.; Perry, J. W.; Barlow, S.; Hu, Z.; McCord-Maughon, D.; Parker, T. C., Ro1ckel, H.; Thayumanavan, S; Marder, S. R.; Beljonne, D.; Brédas, J.-L. *J. Am. Chem. Soc.* **2000**, *122*, 9500−9510.

(21) (a) Dick, B.; Hochstrasser, R. M.; Trommsdroff, H. P. *Resonant Molecular Optics in Nonlinear Properties of Organic Molecules and Crystals*; Vol. 2, p 159. (b) Drobizhev, M.; Karotki, A.; Kruk, M.; Krivokapic, A.; Anderson, H. L.; Rebane, A. *Chem. Phys. Lett.* **2003**, *370*, 690.

(22) Terenziani, F.; Mongin, O.; Katan, C.; Bhatthula, B. K. G.; Blanchard-Desce, M. *Chem.—Eur. J.* **2006**, *12*, 3089.

(23) (a) Oulianov, D.; Tomov, I.; Dvornikov, A.; Rentzepis, P. *Opt. Commun.* **2001**, *191*, 235. (b) Wang, C.; Tai, O.-H.; Wang, Y.; Tsai, T.; Chang, N. *J. Chem. Phys.* **2005**, *122*, 084509. (c) Kauert, M.; Stoller, P. C.; Frenz, M.; Rièka, J. *Opt. Express* **2006**, *14*, 8434.

(24) Prior, Y. *IEEE J. Quantum Electron.* **1984**, *37*, QE-20.